On-board CBCT/CBDT for Image-Guided Proton Therapy: Initial Performance Evaluation

Min Kook Cho[a], Jin Sung Kim[b], Hanbean Youn[a], Sung Yong Park[c], Seungryong Cho[d], Ho Kyung Kim[a *]
[a] *School of Mechanical Engineering, Pusan National University, Busan 609-735, South Korea*
[b] *Department of Radiation Oncology, Samsung Medical Center, Seoul 135-710, South Korea*
[c] *Proton Therapy Center, National Cancer Center, Goyang 411-769, South Korea*
[d] *Department of Radiology, University of Chicago, Chicago, Illinois 60637, USA*
[*] *Corresponding author: hokyung@pnu.edu*

1. Introduction

The advantage of proton beams relative to photon beams for radiation therapy lies in their superior dose-distribution characteristics due to the Bragg peak[1]. In proton-beam therapy, a prescribed radiation dose needs to be accurately delivered to a tumor region minimizing the dose to surrounding normal tissue and healthy organs which are at risk. The high accuracy of patient positioning serves to ensure the geometry and reproducibility of patient positioning. Currently, only two orthogonal x-ray projection images are used to register position of patient at treatment with that of radiation therapy planning (RTP) system in the proton therapy[2]. If CT (computed tomography) images of a patient can be directly acquired in the treatment room, it is possible to compare with CT images of the RTP system, which gives us much more accurate registration results than the conventional orthogonal alignment system. The purpose of this study is to investigate the feasibility of CBCT (cone-beam CT) and/or CBDT (cone-beam digital tomosynthesis) technologies in the treatment room for accurately aligning the patient in the proton beam.

2. Methods and Results

2.1 System description

In the gantry treatment room for proton therapy at the National Cancer Center (NCC), two pairs of x-ray imaging systems (x-ray tubes and large-area flat-panel detectors) are installed in orthogonal directions, as shown in Fig. 1, for the purpose of patient positioning with a prescribed position from planning CT data. In this set, the x-ray tube (A2777, Varian Medical Systems, Inc., USA) is embedded inside the proton-beam nozzle. The detector (PaxScan 4030E, Varian Medical Systems, Inc., USA) is based on arrays of hydrogenated amorphous silicon (*a*-Si:H) thin-film transistors (TFTs) in combination with *a*-Si:H photodiodes, and the overlying phosphor screen.

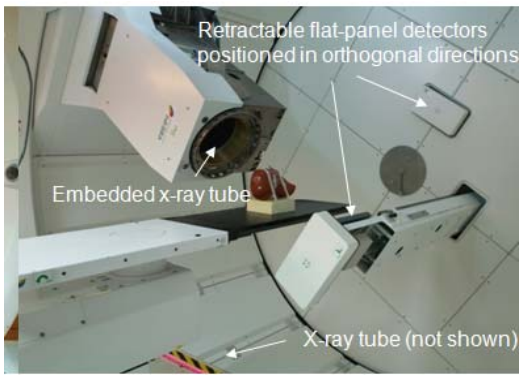

Fig. 1. Proton-beam therapy system in which two pairs of x-ray projection systems are equipped in orthogonal directions for patient positioning.

2.2 Geometric calibration

To determine geometric parameters, such as the source-to-detector distance and tilted angles of the detector, we employed the analytic algorithm and corresponding calibration phantom, which were successfully demonstrated in the megavoltage CBCT system[3]. Based on the measurements of the calibration phantom and analytic algorithm to calculate phantom trajectories, the tilted angles of the detector were analyzed during gantry rotation. The trajectory of the source and detector was evaluated and the excursion was well within 0.5 mm. The distances from the x-ray source to the gantry isocenter and from the detector to the isocenter were estimated to 1517.50 mm and 591.12 mm with a variation of 12 mm or less, respectively.

2.3 Cone-beam computed tomography

For image reconstruction, we employed the Feldkamp's cone-beam algorithm to the projection data filtered with a Ram-Lak filter[4]. The Feldkamp's algorithm is a simple extended version of the conventional filtered backprojection (FBP) method in longitudinal direction by considering cone angles. For acquiring CBCT data, the humanoid phantom was scanned with a rotational angle step of 2° at 85 kVp and 40 mAs. The reconstructed three-dimensional (3D) image format was 512^3 voxels with an isotropic voxel size of 0.4 mm. For the quantitative analysis of CBCT performance, the AAPM CT QC phantom[5] was also scanned at 85 kVp and 40 mAs.

Fig. 2 summarizes the CBCT performances measured

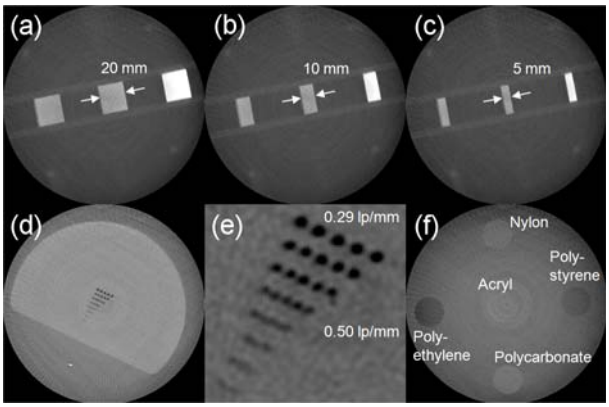

Fig. 2. Reconstructed images for the AAPM CT QC phantom. (a), (b) and (c) confirms slice thickness. (d) and (e) show the resolution hole patterns. (f) is a transaxial image of the low-contrast inserts.

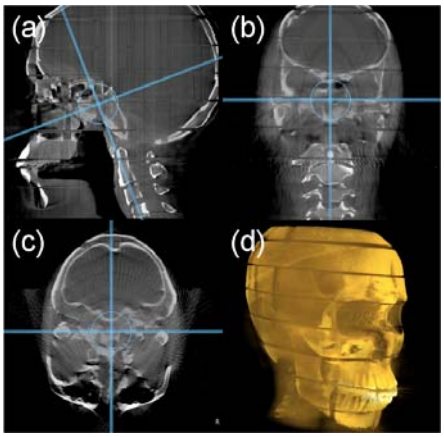

Fig. 3. (a) Sagittal, (b) oblique coronal, (c) transaxial, and (d) volumetric rendering demonstrating CBCT image quality over the volumetric field of view of skull phantom (20^3 cm^3).

with the quantitative AAPM phantom. The plate thicknesses as shown in Fig. 2(a), (b) and (c) describe the slice thicknesses of the reconstructed images. The worst error was ~2.8% for a 5-mm-thick slice. Fig. 2(d) shows the reconstructed image of the hole arrays describing spatial resolution. As shown in the enlarged image of Fig. 2(e), we can distinguish the hole patterns arranged in up to 0.5 lp/mm. The reconstructed low-contrast inserts embedded in water is shown in Fig. 2(f), and which was used for the Hounsfield Unit (HU) calibration. After calibration, the largest error was observed for the insert material of nylon by 3.5%. From the background water region, we measured the SNR of ~20. The CNR between the inserts and the background water was also calculated and the best CNR was 2.54 (polycarbonate) and the worst CNR was 1.14 (acrylic). Fig. 3 demonstrates the CBCT images reconstructed with the humanoid skull phantom. Fig. 3(a) and (b) are sagittal and transaxial views, respectively. Fig. 3(c) is an oblique coronal view along the line designated in Fig. 3(a). The surface-rendered view is demonstrated in Fig. 3(d).

2.4 Tomosynthesis

The theoretical framework for digital tomosynthesis is based on the work of Lauritsch and Härer[6] that reported an FBP method in circular geometry. We employed the combination filter[7] with the angular weighted ramp filter for the scan angle $\pm\alpha$, spectral apodizing filter to control high-frequency noise in the use of the ramp filter and slice profile filter to suppress the frequency response of the out-of-plane blurring structures. For the implementation of both apodizing filters, we used a Hann window function known as a raised cosine window[8].

Comparisons of slice images reconstructed by various approaches are shown in Fig. 3. Fig. 3(a) is a sagittal view of CBCT with 180 projections scanned for 360°. Fig. 3(b) and (c) are images obtained by digital tomosynthesis; the simple shift-and-add (SAA)[9] and FBP methods, respectively, with 21 projections for a 40° scan. While CBDT image using the SAA method exhibits a very blurred image as expected, the CBDT based on the FBP method provides a comparable quality to the CBCT image. The image sharpness of CBDT is preferred to that of CBCT.

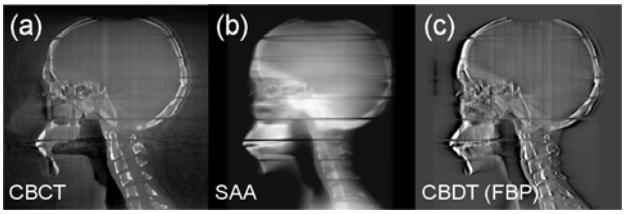

Fig. 4. Comparisons of slice images reconstructed by various approaches. (a) CBCT, (b) SAA and (c) CBDT.

3. Conclusions

CBCT/CBDT for image-guided radiation therapy has been developed and currently practically utilized. However, there has been very little attention paid to proton therapy. In this study, we have investigated the feasibility of CBCT/CBDT for image-guided proton therapy. From the reconstructed phantom images, the CBCT system in the gantry treatment room will be very useful as a primary patient alignment system for image-guided proton therapy. The CBDT may provide fast patient positioning with less motion artifact and patient dose.

ACKNOWLEDGEMENTS

This work was supported by the National Cancer Center Grant (NCC-0810210) and the Korea Science and Engineering Foundation (KOSEF) grant funded by the Korea government (MEST) (R01-2006-000-10233-0).

REFERENCES

[1] A. Smith, "Proton therapy," Phys. Med. Biol. 51(13), R491-R504, 2006.

[2] A. Sawada, K. Yoda, M. Numano, Y. Futami, H. Yamashita, S. Murayama, and H. Tsugami, "Patient positioning method based on binary image correlation between two edge images for proton-beam radiation therapy," Med. Phys. 32(10), 3106-3111, 2005.

[3] Y. Cho, D.J. Moseley, J.H. Siewerdsen, and D.A. Jaffray, "Accurate technique for complete geometric calibration of cone-beam computed tomography systems," Med. Phys. 32(4), 968-983, 2005.

[4] L.A. Feldkamp, L.C. Davis, and J.W. Kress, "Practical cone-beam algorithm," J. Opt. Soc. Am. A 1(6), 612-619, 1984.

[5] P.F. Judy, S. Balter, D. Bassano, E.C. McCullough, J.T. Payne, and L. Rothenberg, *Phantoms for performance evaluation and quality assurance of CT scanners*, AAPM, Report No. 1, 1977.

[6] C. Lauritsch, and W.H. Härer, "A theoretical framework for filtered backprojection in tomosynthesis," Proc. SPIE 3338, 1127-1137, 1998.

[7] M.K. Cho, H.K. Kim, S.-S. Kim, T.W. Kim, S.T. Kim, and S.H Shin, "Development of dental tomosynthesis system," IEEE Nuclear Science Symposium and Medical Imaging Conference, Hawaii, USA, 27 Oct.– 3 Nov. 2007.

[8] F.J. Harris, "On the use of windows for harmonic analysis with the discrete Fourier transform," Proc. IEEE 66(1), 51-83, 1978.

[9] T. Wu, R.H. Moore, E.A. Rafferty, and D.B. Kopans, "A comparison of reconstruction algorithms for breast tomosynthesis," Med. Phys. 31(9), 2636-2647, 2004.